

Article

# Additional Tribological Effect of Laser Surface Texturing and Diamond-Like Carbon Coating for Medium Carbon Steel at Near Room Temperature

Yanhu Zhang <sup>1</sup>, Hao Fu <sup>1</sup>, Xinwei Wang <sup>2,\*</sup>, Hongyu Liang <sup>1</sup>, Julius Caesar Puoza <sup>3</sup> , Jinghu Ji <sup>4</sup>, Xijun Hua <sup>4,\*</sup>, Xiaojing Xu <sup>1</sup> and Yonghong Fu <sup>4,\*</sup>

<sup>1</sup> Institute of Advanced Manufacturing and Modern Equipment Technology, Jiangsu University, Zhenjiang 212013, China; tribo.zhang@gmail.com or zhyh@ujs.edu.cn (Y.Z.); fh0602@sina.com (H.F.); hyliang@ujs.edu.cn (H.L.); xjxu67@ujs.edu.cn (X.X.)

<sup>2</sup> Laboratory for Space Environment and Physical Sciences, Harbin Institute of Technology, Harbin 150080, China

<sup>3</sup> Department of Mechanical Engineering, Sunyani Technical University, P.O. Box 206, Sunyani, Ghana; deokaesar@yahoo.co.uk

<sup>4</sup> School of Mechanical Engineering, Jiangsu University, Zhenjiang 212013, China; jijinghu@ujs.edu.cn

\* Correspondence: xinweiwang@hit.edu.cn (X.W.); xjhua@ujs.edu.cn (X.H.); fyh@ujs.edu.cn (Y.F.)

Received: 30 August 2020; Accepted: 24 September 2020; Published: 28 September 2020



**Abstract:** Texture surface containing both micro-pits and a thin carbon coating was produced using laser surface texturing and magnetic-control vacuum sputtering. Tribological properties of the laser-textured surface coated with thin carbon were experimentally investigated at low-temperature (8–10 °C) under starved and lubricated conditions with a ring-on-ring test rig. The results indicated that the laser-textured surface combined with carbon coating (textured + coating) exhibited low wear intensity and friction coefficient under lubricated conditions, while moderate wear was observed under starved lubrication conditions as compared with the smooth, textured, and carbon-coated surfaces. The wear mechanisms of the lubricated, textured, coated surface under three working conditions (10 N and 1.25 m/s, 16 N and 0.25 m/s, and 50 N and 0.05 m/s) revealed plowing effect, corrosion, and adhesive wear, while oxidative and adhesive wears were observed under starved lubrication. Finally, the textured, coated surface was freely adaptable to different working conditions and exhibited additional effects for better tribological applications at low-temperature as compared with the smooth, laser-textured, and carbon-coated surfaces.

**Keywords:** sliding friction; surface topography; carbon-based coatings; laser surface texturing; low-temperature

## 1. Introduction

Inefficient systemic loss of energy in machinery can be minimized by a reduction of friction and wear in mechanical components [1,2]. For example, the indispensable cogs and bearings in the industrial machine are of interest, with the hope of bridging the gap between our desire for energy and adverse environmental effects [3]. Tribology design and surface engineering technologies are sought after for improving the effectiveness and reducing friction losses in mechanical systems. Available literature indicates that surface texturing is one potential strategy to improve energy efficiency and decrease waste disposal and emissions [2,4]. Textured surfaces, with some intricate microstructures (pits, craters, and grooves), have gained widespread acceptance in tribology because of their ability to achieve the micro-hydrodynamic bearing effect, acting as reservoirs for the continuous supply of

lubricants, and trapping of wear debris by eliminating or reducing plowing effects of the working surfaces [5,6].

Among the surface texture fabrication techniques, laser surface texturing (LST) has become an established manufacturing method [7], owing to its advantages of being extremely fast, clean to the environment, and provides excellent control on shape and size of micro-structures [8–11]. It has been proved that LST is valid for tribological applications in mechanical face seal [12,13], thrust bearings [14,15], cutting tools [16–18], cams/tappets [19], drill bit [20], and piston rings [9,21,22]. LST is also used for the reduction of friction (or stiction) in magnetic storage devices [23] and for the minimization of wear and mechanical losses for micro-electro-mechanical system (MEMS) devices [24]. However, LST is deficient in the new challenges of improving the performances of tribological systems. Importantly, it fails to timely exhibit good transitional process from boundary (and dry) lubrication to full-film lubrication, or vice-versa, though the true state of the tribological system is complicated and filled with uncertainties. An important but little-known problem is the friction and wear mechanisms of textured surfaces with different lubrication regions, as well as effective measures to improve the transitional behavior in various lubrication regimes. LST can increase the range of hydrodynamic lubrication regime in the Stribeck curve [25,26]. Meanwhile, it is stated that the bulges at the edge of the dimple need to be optimized to have the positive effect of LST on lubrication regime transitions [27]. The friction coefficient is an important parameter for tribological performance, followed by wear loss, friction force, efficiency, and reliability, which are all critical to the operation of a special tribological system. In addition, it is necessary to understand the detailed wear and durability of laser-textured surfaces for different regions and working conditions.

Sputtered carbon coatings have been reported to have excellent tribological properties and, therefore, have the potential to be used as a hard solid lubricant and wear-resistant coatings [28]. The coating film is recommended for laboratories and plants for their overt properties, such as chemical stability, morphology, and anti-friction. Specifically, coated surfaces have been amenable to playing an active role in dry friction cases for several decades [29,30]. There is limited literature about the exaltation of tribological performances using appropriate coating film, under mixed film lubrication and boundary lubrication. Though some investigations have shown that carbon film is perfect and can offer a series of attractive properties for many applications [31–33]. Arslan et al. [34] reported two approaches to generate low-wear surfaces with diamond-like carbon (DLC) coating by laser surface texturing. Their results suggested that the tribological performance of a cylinder on a coated plate tribo-pair could be enhanced. Yasumaru et al. [35] investigated the tribological properties of DLC films' nanostructured surfaces by femtosecond laser ablation, where a MoS<sub>2</sub> layer on the nanostructured surface improved the friction properties. The creation of small and shallow cavities with a laser lithography technique on a DLC layer has allowed a significant reduction of the friction coefficient of DLC/steel contact [36]. Recently, an interesting investigation by Ding et al. [37] on carbon film with micro-dots has suggested that the influences of laser textures on the tribological performance of amorphous carbon film are strongly dependent on the friction pairs. For instance, LST has not improved the tribological performance of the friction pairs consisting of Si<sub>3</sub>N<sub>4</sub> balls, whereas it is effective for the reduction of friction for the steel ball. Further, the DLC/LST composite specimens can obtain a low friction coefficient, which has been accounted for by the combined action of dimple-induced graphitizing transformation [38].

Previously conducted tribological studies have mostly focused on the suitable room temperature conditions for human beings to the detriment of outdoor industrial equipment (such as ships, kowtows, and wind turbines) that operates below room temperature. For extreme low-temperature conditions, the tribological researches focus on space and cryogenic aspects, which does not encourage technology development and theoretical progress. In the present research work, the tribological properties of the textured surface with thin carbon coating was compared with three different surfaces (smooth surface, laser-textured surface, and carbon-coated surface) under starved and lubricated conditions at below room temperature (8–10 °C). The result provided fundamental insights to guide the design

and analysis of surface textures for wind turbine bearings, precision bearings, and precision actuators in places like northern China, Scandinavia, Alaska, and northern Russia, where temperatures often remain below room temperature for weeks or months during winter.

## 2. Materials and Methods

### 2.1. Preparation and Characterization

The material specimen utilized for the experimentation was industrially available 45 steel. The 45 steel material is used by numerous manufacturing industries for the fabrication of bearing because it has low friction properties. Before the laser surface texturing (LST), the front surfaces of the samples were ultrasonically cleaned with alcohol and polished by a self-created polishing machine with a diamond aerosol spray of W0.5 grid size for 10 min to a surface roughness of  $<0.56 \mu\text{m}$ . During the texturing process, a Q-switch  $\text{Nd}^{3+}$ : YAG laser oscillator of 50 Watts (OWL, New York, USA) was used to modify the pulse. The single pulse interval processing method was utilized, as reported by Fu et al. [39,40], in the laser texturing process. This process can effectively alleviate the negative heat accumulation effect to accomplish proficient, accurate, and controlled laser micro-textures. The working principle of this process is to coordinate the laser pulse with the mechanical movement of the workpiece to make the laser pulse from the same position separated. The laser beam was focused on the surface of the ablated materials at normal incidence (along the Z-axis) using a convex lens with a focal length of 60 mm and a beam spot diameter of  $60 \mu\text{m}$ . The specimen (small ring) was fixed on a three grasping chuck, which was mounted on a motor controlled two-dimensional stage, and the laser head Z was adjusted to a position so that the focus position was 0.

Round dimples were created on the surface of the ring utilizing the single pulse laser for the tribological investigation. The dimples on the surface of the ring specimen were uniformly arranged in a rectangular array with dot pitch  $L_1$  (circumferential space of the micro-pits) and the line pitch  $L_2$  (radial space of the micro-pits) given as  $150 \mu\text{m}$ . The desired micro-pits diameter was  $60 \mu\text{m}$  with the design texture density ( $T_d$ ) of 12.6 %. The lumps or burrs around the edges of the dimples amid the laser texturing process were expelled by a gentle polishing process. It has been tentatively exhibited that these hardened lumps or burrs around the edges of the dimples negatively affect the tribological performance of contacting surfaces [27].

Conventionally, magnetron sputtering is one of the physical vapor deposition (PVD) methods with high deposition rates and low equipment costs [30] employed in surface coating. After the surface texturing, the nano-carbon coating was then deposited on the target surface by the method of magnetron sputtering with an argon plasma using a turbo chromium coater K575 (Quorum Technologies Ltd., Lewes, UK). A flow chart of the carbon sputtering is shown in Figure 1. Four types of surfaces (i.e., smooth, coated, textured, and textured and coated) were processed for the friction and wear test, as illustrated and presented (Figure 2).

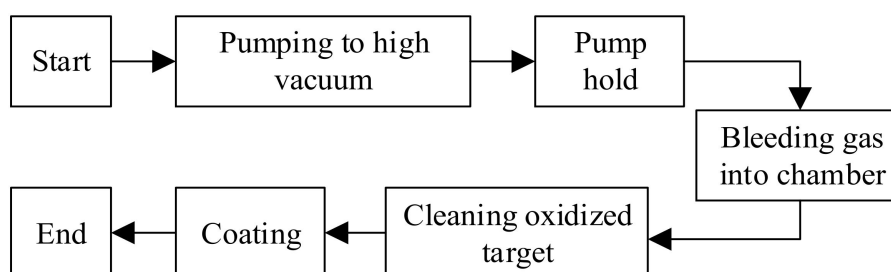


**Figure 1.** Flow diagram of preparation for carbon coating before tribological tests.

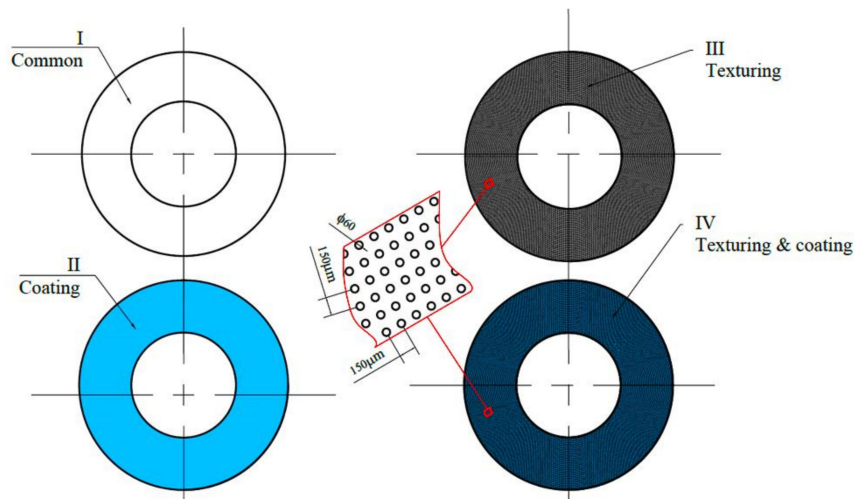


**Figure 2.** Illustration of a smooth surface (I), coated surface (II), textured surface (III), and textured and coated surface (IV).

Surface characterization has spontaneously been one meaningful issue in tribological analysis. The processed surfaces with micro-textures were characterized in 2D parameters and 3D topographies. Abbott curve is widely appreciated by many scientists and engineers, and thus such curves for different surfaces were plotted for comparison. A non-contact optical measuring instrument (WYKO NT1100 of Veeco, Tucson, AZ, USA) was used for the surface topography and characterization (Figure 3).

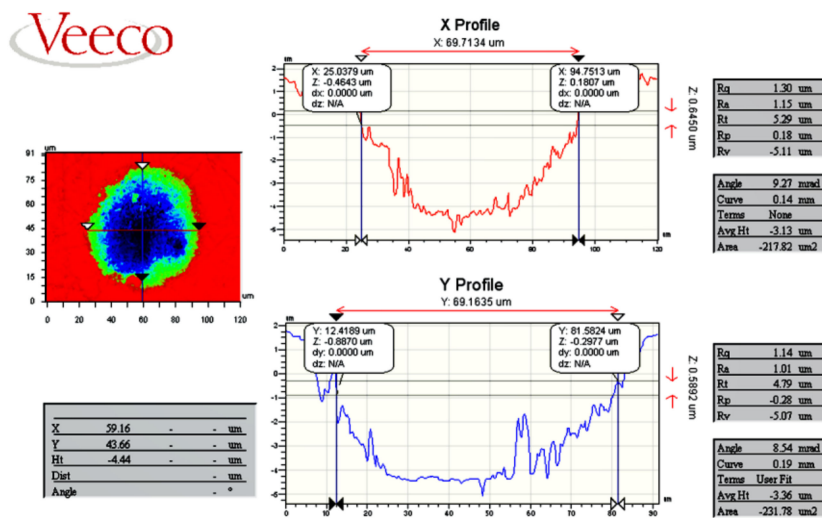


**Figure 3.** Diagram of dimple surface characterization using an optical profilometer.

The bulk 45 steel was finished by quenching in forced air to harden the surface at HRC40~43 and surface roughness of  $R_a < 0.56 \mu\text{m}$ . Dimples of depths 10~15  $\mu\text{m}$  were produced on the surface of the quenched steel to form the textured sample with a roughness value of  $R_a < 0.8 \mu\text{m}$  and hardness value of HRC45~48 after the texturing process. A 0.12  $\mu\text{m}$  thick layer of carbon was then coated on the surface of the quenched 45 steel to form the coated sample with a roughness of  $R_a < 0.5 \mu\text{m}$ . Finally, the quenched textured steel was coated with a 0.12  $\mu\text{m}$  thickness layer of carbon to form a textured, coated sample. The technologies with technical parameters employed in preparing the various surfaces (smooth, LST, coating, LST + coating) for the friction and wear test are given in Table 1. Prior to the friction and wear tests, the contact surfaces of the rings were polished by fine silicon carbide paper (grit number P1000, Shanghai, China) to render the surface finish for all the test specimens at the same level.

**Table 1.** Details of the surface treating process and performance parameters.

Type	Material	Technology	Parameters	Note
Smooth	45# steel *	Quenching; Finishing	$R_a < 0.56 \mu\text{m}$ (L = 120 $\mu\text{m}$ ) HRC 40~43	* parallel to 10455 of ASTM
LST	45#steel; Gas: N <sub>2</sub>	Laser: 512 nm; Nd <sup>3+</sup> :YAG; 50 Watts; 14 Ampere	Space: 150 $\mu\text{m} \times 150 \mu\text{m}$ ; Diameter: 60 $\mu\text{m}$ ; Depth: 10~15 $\mu\text{m}$ ; $R_a < 0.8 \mu\text{m}$ (L = 120 $\mu\text{m}$ ) HRC 45~48	TEM00; Q-switch; Frequency: 6.4 kHz; Pressure: 0.15 Mpa
Coating	45#steel; Target: carbon (TK8869)	Coater: K575; Current: 120 mA; Power: 110 W; Time:12 min	Thickness < 0.12 $\mu\text{m}$ ; $R_a < 0.2 \mu\text{m}$ (L = 120 $\mu\text{m}$ ) HV 1800~2000	Argon: 40 mL/L, 99.99%; Delay: 4 min; No. cycles: 6
LST + coating	45# steel	Same as above	$R_a < 0.5 \mu\text{m}$ (L = 120 $\mu\text{m}$ )	Same as above

Note: "\*" in the table reads that the steel is quenched before experiments.

### 2.2. Tribological Experiments

A configuration of a thrust washer and ring specimen as a friction pair on a whirling rig (MMW-1A, China) was utilized to investigate the tribological performances for the various surfaces, as shown in Figure 4. The upper sample (thrust washer, made of mid-carbon-steel after quenching) was set in the grip holder by a fastening screw. This holder is self-leveling to ensure face-to-face contact during the tests. The lower sample is a circular steel ring with an internal diameter of 16 mm and an external diameter of 32 mm. There are two symmetrically distributed holes on the lower sample for position limitation during the rotation of the principal axis of the testing rig. Besides, there is a small hole on the side surface of the lower sample (2.5 mm from the contact surface) for installing the thermocouple to indirectly test the temperature rise of the contact surface. During the experiment, SC40 (H100) engine oil with the society of automotive engineers (SAE) viscosity of 14.21 mm<sup>2</sup>/s was applied. All the experiments were done at a temperature range of (8–10 °C) and relative humidity of 45 ± 3% for a test duration of 1 h.

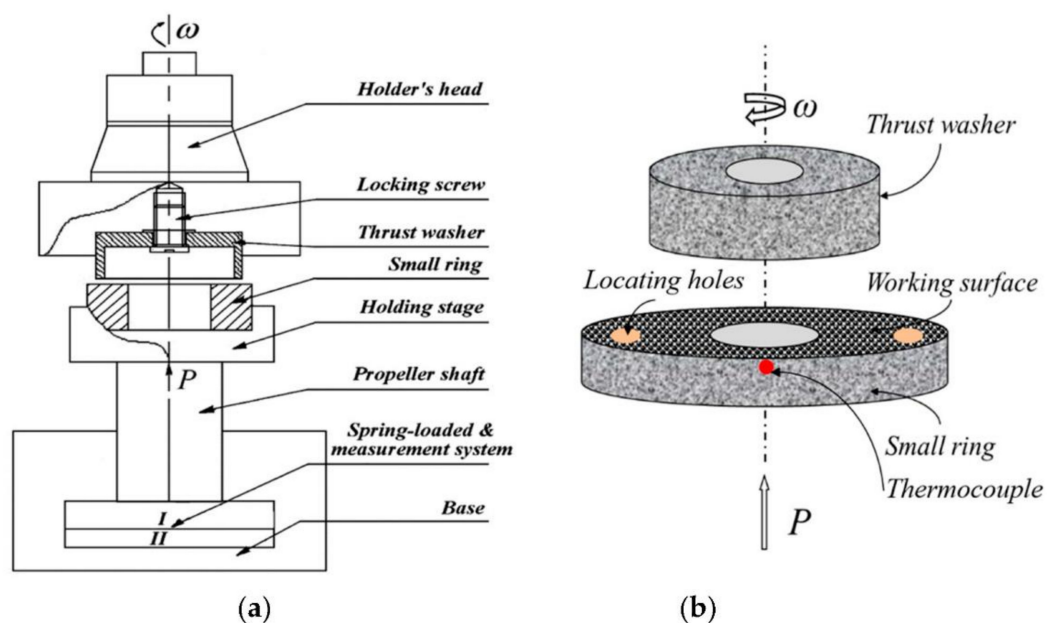


**Figure 4.** Apparatus for tribological tests of (a) the ring-on-ring test rig and (b) friction pair.

Three kinds of PV-values, which reads the load capacity of sliding bearings and is expressed the product of bearing pressure and sliding speed, were examined by the friction test. For simplicity, the bearing pressure was replaced by the normal force  $P$ . The test conditions are presented in Table 2.

**Table 2.** Tribo-test conditions referring to ASTM D3702-94 (R99).

Conditions	Speed (m/s)	Load (N)	Temperature (°C)	Humidity (%)	Viscosity (mm <sup>2</sup> /s)
(PV) <sub>1</sub>	1.25	10	8~10	45 ± 3%	14.21
(PV) <sub>2</sub>	0.25	16	8~10	45 ± 3%	14.21
(PV) <sub>3</sub>	0.05	50	8~10	45 ± 3%	14.21

Note: (PV)<sub>*i*</sub> (*i* = 1, 2, 3) show three typical loading conditions of friction couples, that is, high-speed and light-load condition, middle-speed and middle-load condition, and low-speed and heavy load condition.

During the experiments, the normal load  $P$  and friction torque  $T_f$  were recorded simultaneously to determine the coefficient of friction. The friction coefficient of the small thrust washer-ring pair was derived as follows.

$$f = F/P = T_f/(R_s \cdot P) \quad (1)$$

where  $F$  is the frictional force,  $R_s$  is the equivalent contact radius of the ring given by  $R_s = (d_1 + d_2)/4$ .  $d_1$  and  $d_2$  are the external and internal radius of the ring, respectively. Wear behaviors of the surfaces were evaluated by combining both qualitative and quantitative methods. The wear intensity  $I_w$  as an index was interpreted by expression (2).

$$I_w = \Delta m / [(P/A_a) \cdot L] \quad (2)$$

where  $\Delta m$  is the change in mass of the specimen before and after the friction test. The values were obtained by reading from an electric balance scale (Ohaus discovery, semi-micro, and analytical balances with 10 microgram readability).  $P$  is the normal load,  $A_a$  is the apparent area of contact during sliding, calculated from  $A_a = \pi(d_1^2 - d_2^2)/4$ , and  $L$  is the sliding distance during the whole test duration. The friction and wear test of each condition was repeated three times, and the average values were presented to ensure the repeatability of the results.

### 3. Results

#### 3.1. Surface Characterization

Through analysis and comparison, a compound characterization of the 2D critical parameters and 3D topographies are presented. The  $R_a$  gives a general description of the surface amplitude, and  $R_q$  means the average of the measured height deviations taken within the evaluation length of the area. They are meant for traditional characterization in tribological applications. Specifically, they are critical in illustrating the friction stability and wear resistance.  $R_t$  is very sensitive to large deviations from the mean line and from scratches and also reads the uniformity of the surface roughness. In addition,  $R_{pk}$  indicates the top portion of the surface that is worn away in the run-in period, and  $R_{vk}$  reads the lowest part of the surface that retains the lubricant. Furthermore, the values of bearing ratios obtained from the bearing ratio curve (Abbott–Firestone curve) are  $M_{r1}$  and  $M_{r2}$ . The ideal value of  $M_{r1}$  is small, while the value of  $M_{r2}$  is large. After the analysis of the measured results, some useful parameters obtained are presented in Table 3. The surface characterization of the smooth surface is illustrated in Figure 5. It is observed that the smooth surface has a uniform roughness in horizontal and vertical directions, although it has a different waviness and texture after the characterization of the surface parameters. The Abbott–Firestone curve further supports this illustration for the bearing ratios of two sections ( $S_1$  and  $S_3$ ), which present a high consistency. The laser-textured surface has a higher roughness as compared with the smooth surface. Inversely, the surface roughness of the coated surface is lower than the smooth surface. The coated surface has the lowest roughness parameters ( $R_a$ ,  $R_q$ ,

$R_t$ ,  $R_{pk}$ ,  $R_{vk}$ ), while the textured surface has the highest roughness. The textured surface has a higher value of  $R_{vk}$  than the other surfaces. These values reveal that a given surface has excellent properties of abrasive resistance under uniform materials and working conditions.

**Table 3.** Roughness and Abbott–Firestone parameters of different surfaces before wear tests.

Parameters	Smooth	Textured	Coated	Textured + Coated
$R_t$ ( $\mu\text{m}$ )	12.45	11.51	4.32	9.45
$R_a$ ( $\mu\text{m}$ )	0.553	0.705	0.126	0.404
$R_q$ ( $\mu\text{m}$ )	0.700	1.130	0.177	0.593
$R_{pk}$ ( $\mu\text{m}$ )	0.592	0.728	0.154	1.287
$R_{vk}$ ( $\mu\text{m}$ )	0.945	3.321	0.329	0.487
$V_1$ (nm)	21.29	17.36	5.75	56.4
$V_2$ (nm)	82.47	375.49	22.36	26.38
$M_{r1}$ (%)	7.19	4.76	7.47	8.76
$M_{r2}$ (%)	82.56	77.38	86.42	89.17

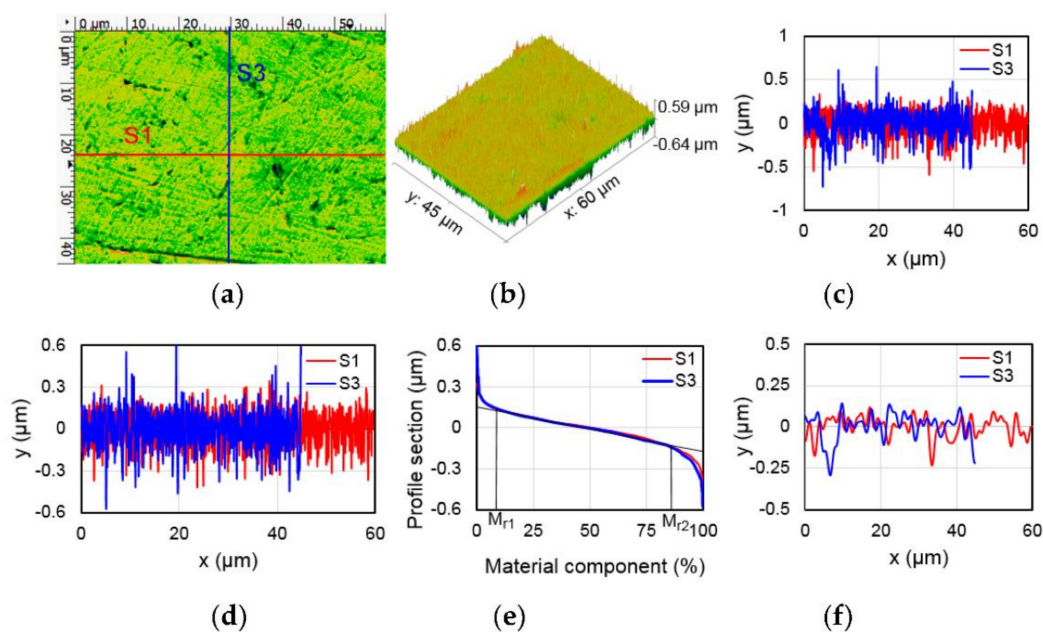


**Figure 5.** Surface characterization of the smooth surface of (a) 2D topography, (b) 3D topography, (c) texture, (d) roughness, (e) Abbott curve, and (f) waviness.

The working conditions of a friction pair usually change during operation. For comparison of surface topographies and parameters against the working conditions, three-dimensional topographies of the laser-textured surface with coating are presented after the wear tests under lubricated and starved conditions, respectively (Figures 6 and 7). The wear traces of the laser-textured surface with a coating under lubrication is clear and shallow. The asperity contact undergoes a light load, and the friction pair forms hydrodynamic lubrication. The surface roughness is rather high after the wear test. This means a laser-textured surface with the coating is reliable and durable for lubrication conditions. Abbott curves showing the coincidence of cross-sections (S1 and S2, Figure 7) direct that the wear loss of the non-textured regions is isotropic in the horizontal and vertical directions. The peak region of the worn away section of S3 is larger than that of the S1 and S2, while the core region of S3 is less than S1 and S2. This means the vertical asperities cannot bear the large load, and the life of the friction pair is short. However, the valley region acts as a lubricant reservoir ( $S3 > S1, S2$ ).

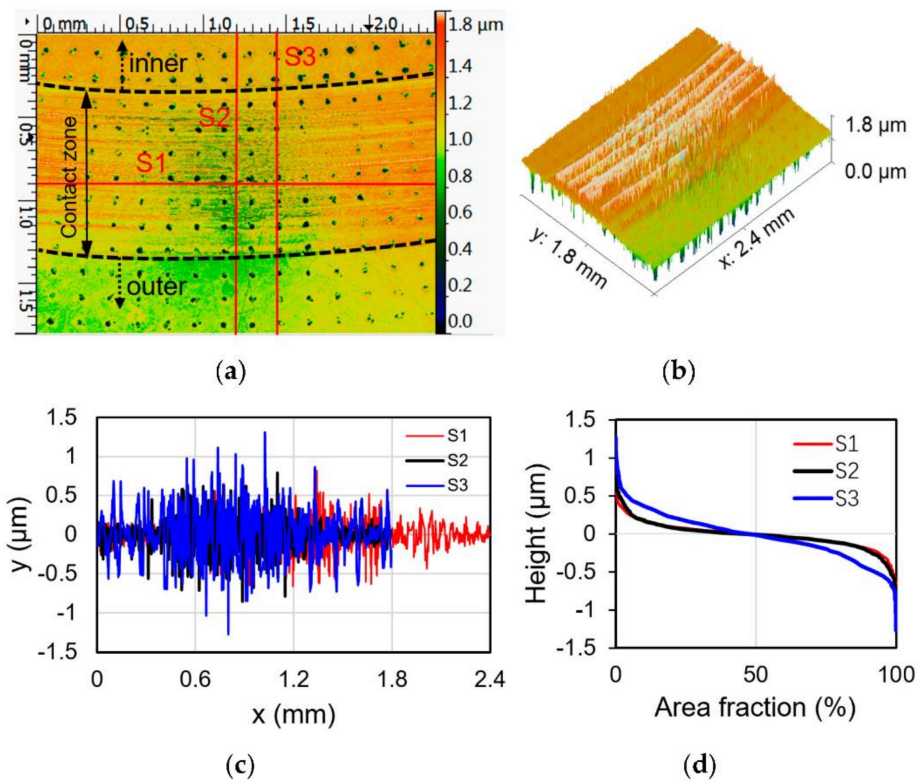


**Figure 6.** Surface characterization of the laser-textured and coated surface after wear test with 2D topography (a), 3D topography (b), section contour (c), Abbott curve (d) ((PV)<sub>2</sub>: lubrication).

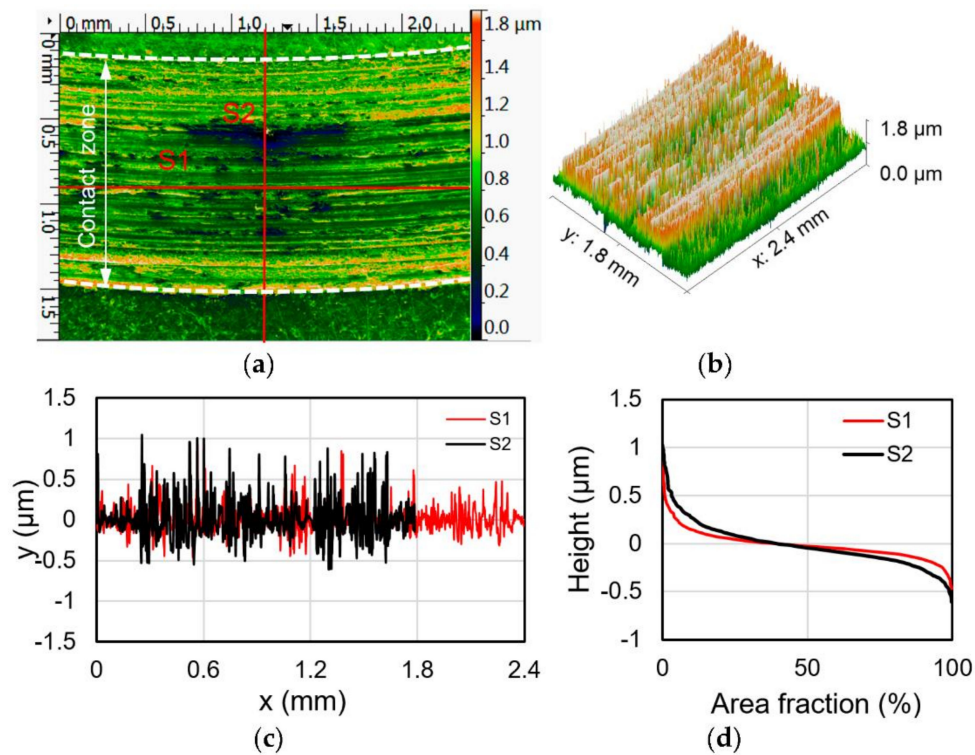


**Figure 7.** Surface characterization of the laser-textured and coated surface after wear test ((PV)<sub>2</sub>: starvation): (a) 2D topography, (b) 3D topography, (c) section contour, (d) Abbott curve.

The wear trace width under lubrication is about 1 mm, whereas the width of the wear trace under starvation is about 1.35 mm. The roughness of the worn surface under starvation is lower than that of lubrication. The valley of the worn surface under starvation is shallow, which is due to the wear debris filling and the surface material flow during abrasive wear. In addition, the worn surface under starvation presents a complicated topography, which may be related to complicated wear mechanisms. Firstly, there is no lubricating medium between the friction pair, which can produce the so-called hydrodynamic lubrication and bearing force under dry friction. Importantly, the asperities of the friction pair on the LST surface are directly in contact, and the contact area is fairly small, resulting in high contact stress, which induces material deformation of the metal subsurface and the non-textured regions. Secondly, it is still the metal matrix material that plays a supporting role, although thin DLC coating on the contact surface. Under direct contact and shear action of the friction pair, material migration and accumulation deformation occur, and contact hot spots are formed in the rough friction area to cause local oxidation.

### 3.2. Friction Properties

The coefficients of friction of the different working surfaces are measured through friction tests, and the comparison is shown in Figure 8a. The smooth surface exhibits the highest friction coefficient and shows sustainable growth over the initial test period. The textured surface induced by the laser presents a stable friction coefficient trend during the test period. The laser texturing has some effects on the stable friction coefficient. The first aspect is the quenching effect and refinement of microstructure for a high quenching rate [41], which increases the surface hardness of the sample [42] and improves the abrasive resistance. According to the molecular-kinetic and mechanical model theories of the frictional behavior of elastic materials, the magnitude of the friction coefficient is inversely proportional to the hardness of steel surfaces [43]. The induced quenching effect by the laser increases the amount of martensite phase, which effectively decreases the surface friction coefficient and, consequently, improves the surface wear resistance. Secondly, the debris collection by the micro-pits hinders the attendance of the so-called third-body wear between the friction pair. Finally, the laser-material interaction on the surfaces and interfaces during the texturing process will result in recombination actions of the steel structure, which alter the surface chemistry, morphology, and crystal structure of the steel to form a new material structure with better tribological properties.

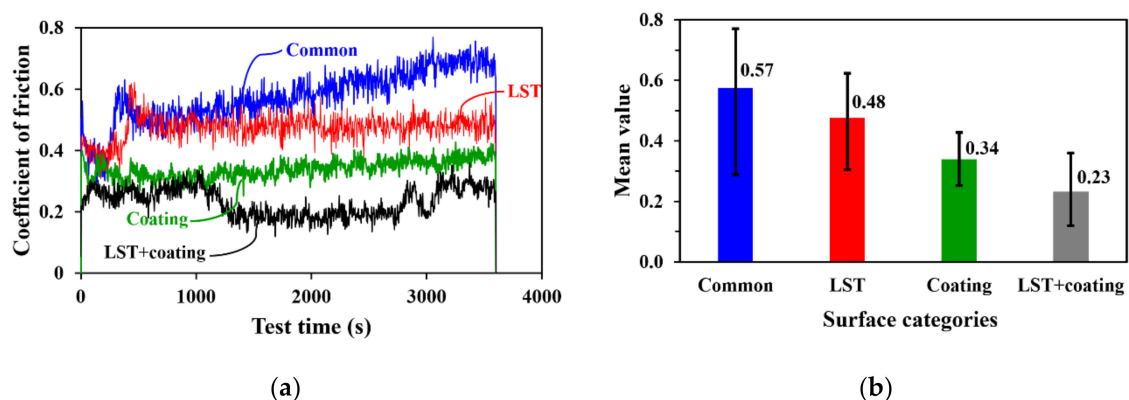


**Figure 8.** Friction coefficient vs. the sliding time (a) and the mean values (b) for four categories of surfaces under lubricated conditions at  $(PV)_2$ , i.e.,  $P = 16$  N,  $v = 0.25$  m/s.

The carbon-coated surface exhibits a low friction coefficient as compared to the smooth and textured surface regardless of the test time. This is because of the carbon coating layer and the special full harden and steel surface through laser quenching. However, the friction coefficient shows a slowly growing trend. This might well be due to the failure of the carbon coating. Carbon coatings affect the plowing component of friction, while rough surfaces affect the degree of asperity penetration through

the coating into the substrate [44]. In addition, diamond-like carbon has an amorphous lattice structure, with  $sp^3$ ,  $sp^2$ , and  $sp$  bonding type coexisting, and the hardness varies from 1500 HV to 6000 HV [45]. All of these make the phase transformation occurs easily when the local temperature gets up to 250 °C or even higher; graphitization is an unexpected result [46]. However, the changes in the carbon films' properties are beyond the recognition of engineering problems.

The friction coefficient of the textured surface with carbon coating shows more than one steady phase for the test duration. At the beginning of the test, the coefficient of friction shows a modest growing tendency. After 15 min, it goes into a steady-state with a considerable low value of about 0.17 for 20 min. The friction coefficient then passes into another steady-state after around 10 min. Theoretically, the friction binomial law indicates that the friction coefficient consists of two components. One is the mechanical interaction of the friction pair asperities on the macroscopic level, and the other is the molecular action of the surface film on the nanosomic scale. The in-depth mechanism of these components is considered in the analysis of the tribological performance. Laser surface texturing (LST) has a macro sense compared with the carbon thin film embedded on the flat surface. An attempt is made to search for a better tribological performance from a physiochemical standpoint. However, the result cannot fit comfortably with the superimposition of mechanical and molecular interpretation in this study because the water molecules play a prominent role in the frictional behavior of DLC films [47]. The friction coefficient of the four different samples in increasing order is as follows: textured + coating (0.2327), coating (0.339), textured (0.4746), and smooth (0.5744), as indicated in Figure 8b. Comparing with the smooth surface, the friction coefficient of textured, coated, and textured + coated surfaces are reduced by 17%, 41%, and 59%, respectively.

The curves of the friction coefficients for the textured surface with carbon-coated film for different working conditions are plotted in Figure 9a. In addition, the steady-state values are shown in, which are the average of the steady-state portion of the actual friction coefficient. The adulatory curve of friction coefficient provides a particularly sensitive monitor to an imperfect aspect of the carbon coating film. The data reveals that the coefficient of friction is fairly low under low-speed and heavy load conditions, referred to as  $(PV)_3$ . The value is hardly higher than 0.2, but for the transitory fluctuation, it has resulted from the mechanical inertia of the test rig. The comparison test suggests a greatly higher value of friction coefficient for the whole duration under high-speed and lightly loaded conditions, referred to as  $(PV)_1$ . However, it has a pretty good tendency to decrease following the test time. It is, therefore, easy to conclude that the textured surface with coated carbon thin film investigated in this study has a desirable performance under low-speed and heavy-load conditions in boundary lubrication for most engineering problems. For example, a piston in an internal combustion engine gets to the top dead center or bottom when the speed is very low, but carrying a heavy load. As discussed above, the coefficient of friction under the conditions of mid-velocity and moderate load, referred to as  $(PV)_2$ , shows a phased fluctuation, which may be due to the so-called three-body abrasion. During the rest, there may be some generation, variation, and transfer of abrasive particles, which are moving from one subdomain to another and change with the occurrence of squeezing effect and surface deformation. The temperature diachronic curve obtained by using a thermocouple sensor arranged in the side hole of the thrust ring specimen is shown in Figure 9b. Considering the same material matrix, it can be considered that the temperature diachronic curve is an indirect measurement result of the friction temperature rise. It can also be seen that the friction temperature rise is closely related to the working conditions. In the initial stage, the friction temperature rise is lower at low and high-speed conditions (i.e.,  $(PV)_1$ ,  $(PV)_3$ ) and then increases to a higher degree (about 3 min). Interestingly, the temperature rise curve corresponding to working condition  $(PV)_2$  is relatively high at the initial stage and then remains stable, which is different from the other two conditions. This indirectly reflects that the textured surface with carbon coating has good adaptability and application for medium-speed and medium-load conditions.

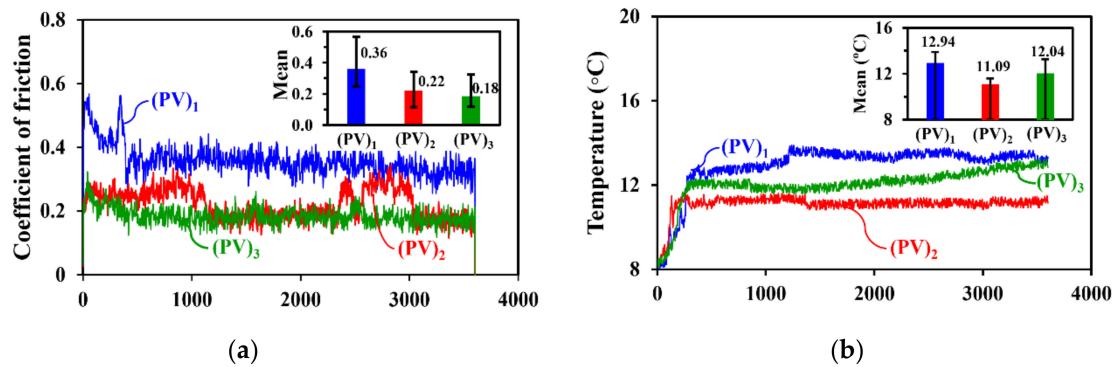


**Figure 9.** Friction coefficient curves (a) and temperature diachronic curves (b) for the laser-textured surfaces with carbon coating under lubricated conditions at (PV)<sub>1</sub>, (PV)<sub>2</sub>, and (PV)<sub>3</sub>. Concretely, that is,  $v = 1.25$  m/s,  $P = 10$  N;  $v = 0.25$  m/s,  $P = 16$  N;  $v = 0.05$  m/s,  $P = 50$  N.

### 3.3. Wear Behavior

For the treated surfaces, a low coefficient of friction alone is insufficient to account for excellent tribological performance. Instead, extended humps for allowing adjacent carbon layers to slip over each other or over contacted material during the rubbing-in process, generally, have good wear-resistance. The wear intensities of the different surfaces are measured by an electronic balance with an accuracy of 0.01 mg, and the results are shown in Table 4 and illustrated graphically in Figure 10. Meanwhile, the wear scratches of the different surfaces under lubricated and starved conditions at different loads and velocities are tracked by SEM photos. To ensure that this is indeed the case, the energy-dispersive spectroscopy (EDS) (0~20 keV accelerating voltages) maps to study the inferred results on wear behaviors and mechanisms for textured and coated surfaces are illustrated. Although there is no significant reinforcement point in the SEM analysis, it is far from being a powerful surface analytical technique.

**Table 4.** Wear intensities for the four categories of surfaces under different test conditions.

Working Condition	Wear Intensity $I_{wr}$ , $\times 10^{-6}$ (mg/N·m)					
	Smooth	Textured	Coated	Textured + Coated		
Lubrication	2.8861	-3.2401	0.0476	0.9277	0.5542	-0.8515
Starvation	0.0959	-3.2742	-3.5881	2.4829	-	-
Note	(PV) <sub>2</sub>	(PV) <sub>2</sub>	(PV) <sub>2</sub>	(PV) <sub>2</sub>	(PV) <sub>3</sub>	(PV) <sub>1</sub>

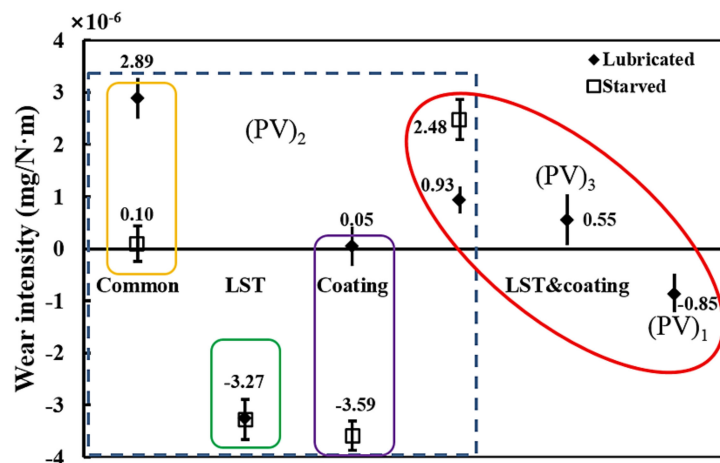


**Figure 10.** Wear intensities for the four categories of surfaces under different conditions.

It is interesting to note that there are differences in the wear loss of the various surfaces, both quantitatively and qualitatively. Firstly, as illustrated in Table 4, there is an increase in wear for the smooth surface, and the wear intensity values are positive. This phenomenon occurs under starved lubrication conditions on the ground that the friction pair consists of homogeneous medium-carbon steel with excellent elasticity in sliding friction. However, under lubricated conditions, the wear has reduced, as the oil film is enough to engulf the asperities and be replaced by viscous drag. The value of the wear intensity under full lubrication is 30 times more than that under starved lubrication conditions. SEM micrographs of worn surfaces of the smooth surfaces in sliding experiments at  $(PV)_2$  are presented in Figures 11a and 12a.

As demonstrated, the plowing component of friction is weakened due to the separation of crests and peaks between the working surfaces by the viscous fluid under the lubricated condition. However, there are micro-cracks in the perpendicular direction of the sliding motion. When two rough surfaces are pressed together, the high pressure will give rise to elastic and plastic deformation at the tips of the surface asperities [48]. The wear patterns suggest that there is an accumulation of material near the two sides of the contact zone on the sliding surface, which may be due to the plastic deformation of the metal materials within the contact interface. The working surfaces embedded with hard particles always produce furrows and grooves in the process of sliding motion under starved conditions. The so-called three-body wear is produced by the two contact surfaces, and the hard particles are detached from the surfaces. As a result, the plowing effect is exacerbated, and the debris cannot stand the overwhelming local pressure other than been crushed at a high friction temperature. Some of the free-form abrasive particles are thereupon transferred timely between the contact surfaces, as indicated in Figure 12b. The tremendous heat from friction provides the right conditions for oxidation wear of the releasing particles during the instantaneous frictional contact with the partial working surface, resulting in the formation of black carbon. Additionally, the hardness of the contact surfaces of the friction pairs is approximately equivalent and prone to create adhesive wear mechanism.

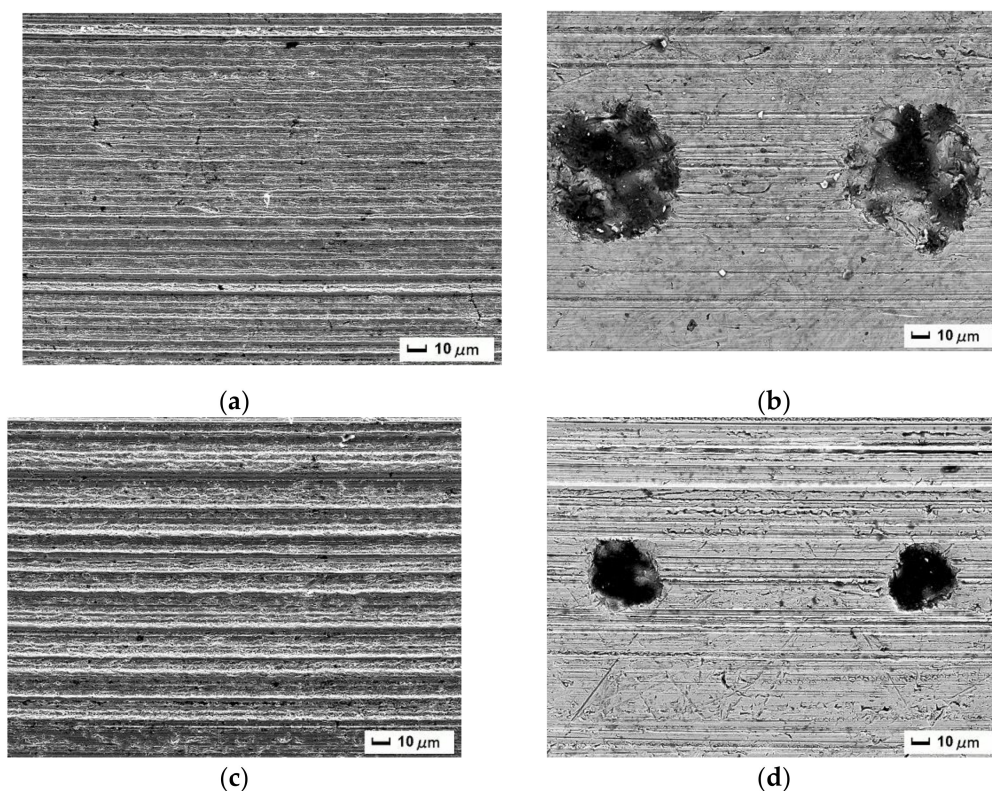


**Figure 11.** SEM micrographs of smooth (a), textured (b), coated (c), and textured + coated (d) worn surfaces under lubricated conditions in the sliding experiments at  $(PV)_2$ , ( $P = 16$  N,  $v = 0.25$  m/s).

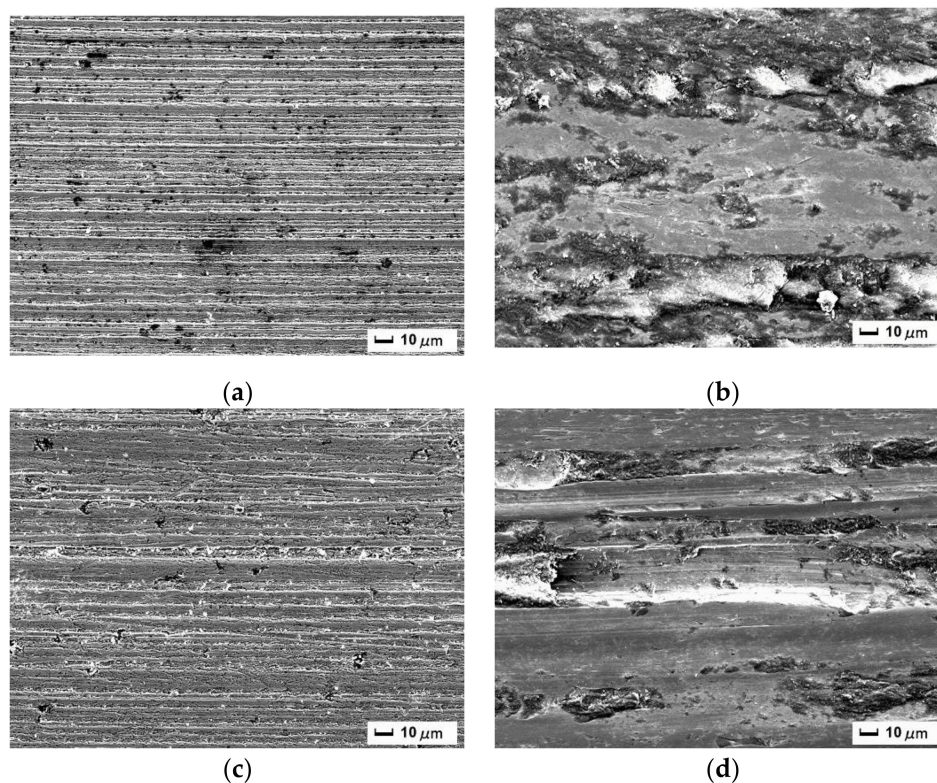


**Figure 12.** SEM micrographs of smooth (a), textured (b), coated (c), and textured + coated (d) worn surfaces under starved lubrication conditions in the sliding experiments at  $(PV)_2$ , ( $P = 16 \text{ N}$ ,  $v = 0.25 \text{ m/s}$ ).

The wear intensity of the textured surface is negative both under lubricated and starved conditions at  $(PV)_2$ , as illustrated in Figure 10. It can be inferred that the abrasive debris lost from the counter body with low surface hardness and adhesive action makes the grains fall into the micro-pits and on the nearby textured surface. SEM micrographs of worn surfaces of the textured surfaces in sliding experiments at  $(PV)_2$  are displayed in Figures 11b and 12b. Under the lubricated conditions, the worn surface reveals light scratches on the textured surface with some free abrasion particles along with the sliding motion. This is attributable to the micro-bearings effects of the micro-pits array. The wear pattern demonstrates that the laser-textured surface has excellent skills to deal with lubricants and debris, with an interesting consequence for tribological behavior during the friction test under lubricated conditions. As presented, the carbon is no longer stable because of the increasing and accumulation of friction heat located in the contact zones under dry and loaded conditions.

Contrarily, the wear intensity of the coated surface under lubricated conditions is not negative. It confirms that carbon film could reduce the hardness of the working surface and then improve the abrasive resistance. Furthermore, the value is much less than the textured surface under the same conditions. SEM micrographs of worn surfaces of the carbon-coated surfaces in the sliding experiments at  $(PV)_2$  are exhibited in Figure 11c. As presented, adhesive wear becomes a predominant mechanism for the carbon-coated surface due to the low surface hardness of the carbon-coated film. Meanwhile, the viscous effect of the lubricants increases evidently due to the wetting mechanism of the carbon film, and the friction increases with the exposed asperities on the counterpart surface. This results in serious wear particles that are turned out under lubricated conditions. As shown in Figure 12c, dissimilarly, carbon film plays the role of solid lubricant during the sliding motion, which actively alleviates the action of asperity-to-asperity contact, and the friction process is no longer uneven with contradictions. Consequently, wear and vibration have been reduced by the carbon thin film and the enclosed particles. However, there exist hard particles as foreign matters stored within the subsurface, which turns out and becomes free debris as soon as the thin carbon coating is worn out.

As suggested in Table 4, under lubricated conditions, there is little difference in the values of wear intensities under different loads and sliding speeds for the textured surface with a carbon coating. By comparison, the wear intensity with positive values  $(PV)_3$  has been the smallest, while  $(PV)_2$  has been the highest. However, under  $(PV)_1$ , the wear intensity is intermediate with a negative value. The wear intensity of the textured, coated surface with micro-pits array is positive, though its values are fairly high. From these values, we can induce that there are different wear mechanisms for the textured surface under different working conditions, as illustrated graphically in Figures 11d, 12d and 13.

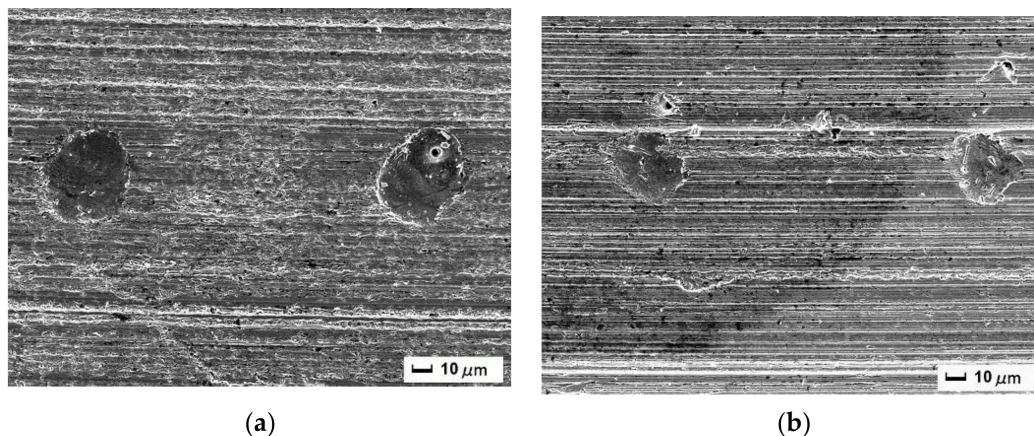


**Figure 13.** SEM micrographs of worn surfaces of the laser-textured surfaces with carbon coating under a lubricated condition in the sliding experiments at (a)  $(PV)_1$  and (b)  $(PV)_3$  for 1 h.

Specifically, the wear tracks on the textured, coated surface under lubrication at  $(PV)_1$  is illustrated in Figure 13a. It shows that the plowing effect under the conditions of the high-speed and light load is not dominant alone, but being accompanied by corrosion and adhesive wear. This may be as a result of the combined micro-plowing, micro-cutting, and micro-cracking mechanisms in the micro-texture during the friction test. The worn tracks on the textured surface with carbon coating under full lubrication at  $(PV)_2$  is expressed in Figure 11d. As seen, shallow and burnished scratches on the friction surface denote that micro-plowing is the predominant wear mechanism. Furthermore, wear traces on the textured surface with coating and micro-pits under lubrication at  $(PV)_3$  is expressed in Figure 13b. On the one hand, the plowing effect is the primary wear mechanism for the friction pair consisting of conformal surfaces; on the other hand, adhesive wear exists as a secondary mechanism. Unlike the preceding results at  $(PV)_2$ , there are wormlike wear particles along the sliding direction. Lastly, the wear tracks under starved conditions are exhibited in Figure 12d, which shows that there are oxidative and adhesive wears. Surprisingly, the micro-textured structure on the bulk material is buried with some deformation.

The energy-dispersive X-ray spectroscopy (EDS) examination spectrums of the novel laser-textured surfaces with carbon coating after the friction tests are presented in Figure 14. There are significant differences in the element intensity in the contact point within the wearable zones after the friction test under different working conditions. Specifically, the iron contents within the textured, coated surfaces decrease variably under different lubrication conditions, but the emerging oxygen seems to present some.

Comparing the three PV conditions under lubrication, the iron content is high under  $(PV)_2$  (Figure 14b) condition but is decreased under  $(PV)_3$  (Figure 14c), while the datum  $(PV)_1$  (Figure 14a) condition does not offer any evident information. For the steel substrate, the decrease in iron content suggests that the friction and wear on the surface material are severe, while the increase in iron content shows that the novel surface is wearable. The added iron content illustrated on the material of the sliding counterpart may be lost and less on the treated surface. There are two illustrations for the causes of the unapparent change of iron content under  $(PV)_1$  condition. One may be that the contact

surfaces of the friction pair are anti-friction. The other may be that the friction pair consisting of the same material has the same physicochemical properties, leading to the dissolution occurring on the contact surfaces of the pairs. It can clearly be seen that these cases are consistent with the results mentioned before the friction test.

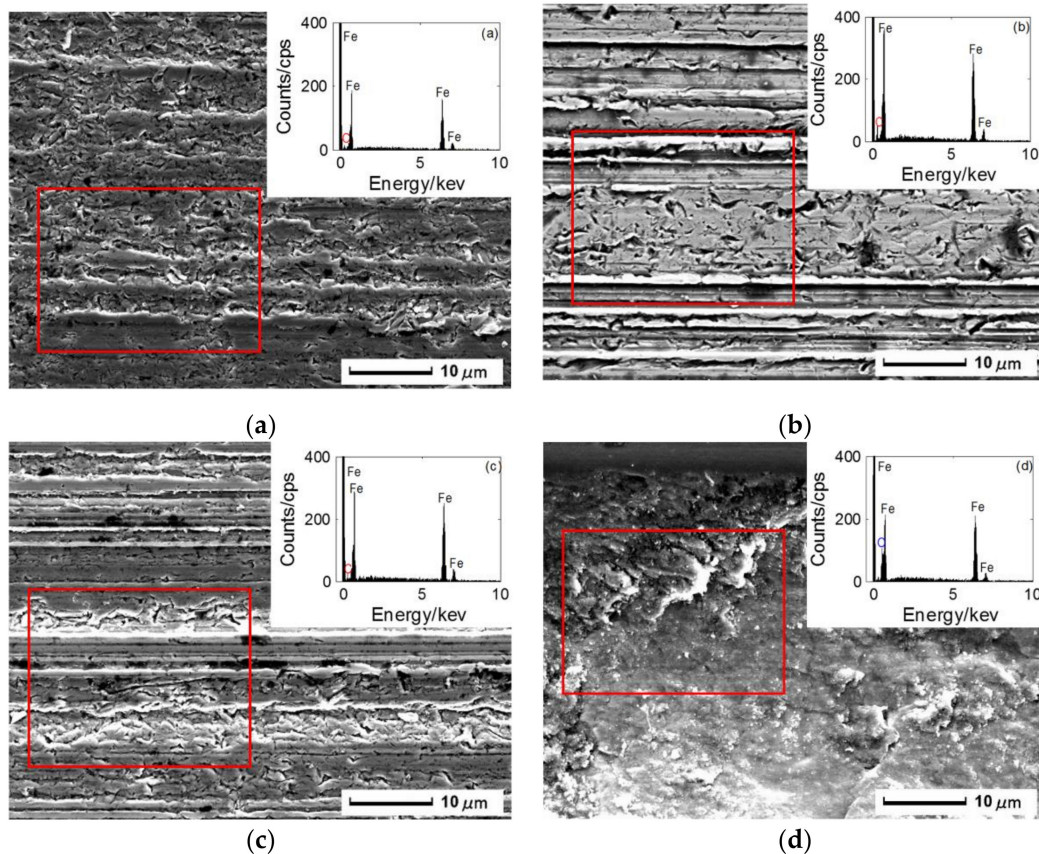


**Figure 14.** Local energy-dispersive X-ray spectroscopy (EDS) maps of the laser-textured surfaces with carbon coating after friction tests at different working conditions: (a) lubrication and (PV)<sub>1</sub>, (b) lubrication and (PV)<sub>2</sub>, (c) lubrication and (PV)<sub>3</sub>, (d) starvation and (PV)<sub>2</sub>.

#### 4. Discussion

In this study, the laser-textured surface with DLC coating displays different tribological behaviors during the friction and wear test, and these behaviors are related to the bulk materials and micro-pits and the DLC-coated layer. Firstly, laser surface texturing can be seen as a partial laser machining on the surface of carbon steel by laser ablation gasification, accompanying laser transformation hardening (also known as laser quenching) [49]. The heating effects of the laser beam need some attention. The heat is absorbed rapidly ( $10^{-1}$ – $10^{-7}$  s) in a small area on the surface of the workpiece, and the temperature rises sharply [50]. The solid phase transformation occurs between the melting point of the material and the critical temperature of austenite transformation. After self-quenching, martensite is obtained, and the transformation hardening of the workpiece surface is realized, resulting in the complete hardening of the 45 steel surface with partially quenched areas. The microstructure consists of fine needle-like martensite [51], although material structure, heating, and cooling speed are important factors for the transformation of hardening behavior [52]. This results in improved strength and hardness of the surface. Specifically, due to the steep temperature field distribution, there is a sharp transition from the laser hardened layer to the matrix and the second characteristic of local diffusion of carbon, and the hardness drop is as high as HV400–600 [50]. Besides the laser nitriding, other recombination actions might well exist during the surface texturing to improve the tribological properties for the nitrogen as

the assist gas during LST processing. The surfaces of the dimples also contribute to improving the tribological properties, especially for the contribution of low and steady friction [53]. Importantly, the hardness of hydrogenated DLC films, which is typically around 10–20 GPa depending on the  $sp^2$  to  $sp^3$  ratio and the hydrogen content, will act as anti-friction and anti-abrasion film [54]. Generally, TK8869, as a target material for carbon coatings, tends to be amorphous carbon material and is accepted as a soft coating for anti-friction and anti-abrasion. Therefore, the DLC carbon coating is adaptive to the boundary lubrication and mixed lubrication conditions for controlling friction and wear. Conclusively, emphasis should be placed on the effect of surface texture and coating on the surface friction properties. Regulation of the friction coefficient and the expansion of the Stribeck curve are available for the novel surface, treating with combined LST and DLC coating. After the tribological experimental data by Kalin et al. [55], the friction coefficients obtained are analyzed, and the results are shown in Figure 15. As shown, the friction coefficients increase initially with the Stribeck parameter and then decrease with a further increase of the parameter in the measurable range. LST and DLC are effective in regulating the behaviors of friction couples under different working conditions. Specifically, LST can expand the contact parameters for hydrodynamic lubrication and induce the friction transition on the Stribeck curve [27]. Meanwhile, DLC coating exhibits comfortable friction properties under boundary lubrication by forming a low friction film on the surface. Additionally, the friction properties can be highly improved by using extreme-pressure and anti-wear additives [56,57]. In this study, the experimental results, by considering the compound influence of LST and DLC coating, are far from that of the literature [55]; they may be accounted for the clear difference in the initial surface roughness and lubrication oil. However, compared with the LST surfaces, friction transitions occur on the Stribeck curve of the novel design LST surfaces with DLC coating.

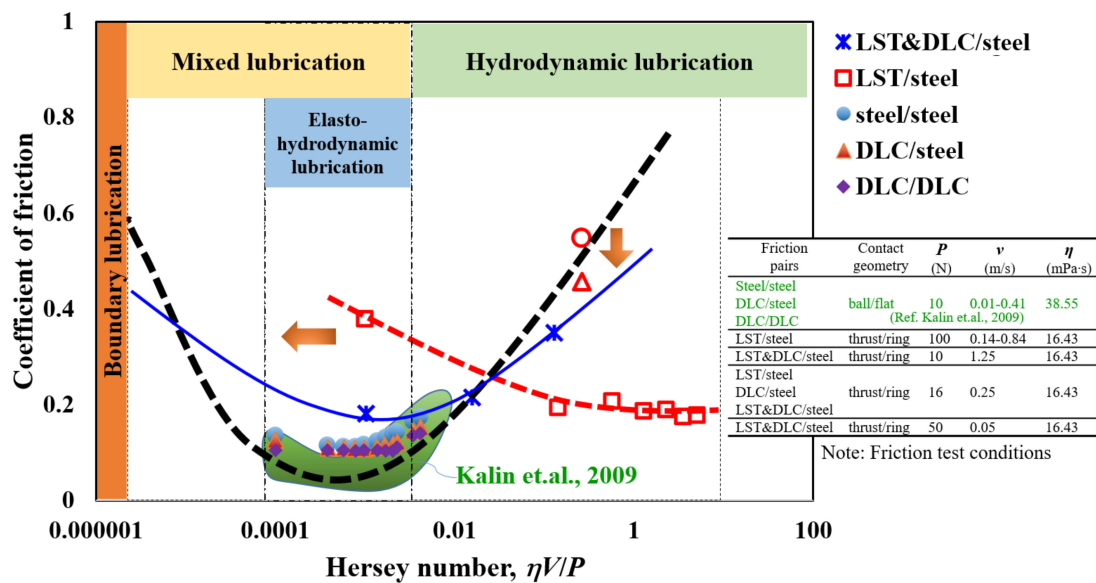


Figure 15. Illustration of the expansion of the Stribeck curve by laser surface texturing (LST) and diamond-like carbon (DLC) coating.

Wear mechanisms of LST surface with carbon coating is complicated for the given full-range lubrication and friction conditions. After the transformation of hardening through the LST process, the occurred grain refinement can improve the plastic deformation resistance and fracture strength, increase the stress caused by cracks, and increase the wear resistance [50]. Meanwhile, the DLC film is acknowledged for the low friction coefficient, good wear resistance, and high hardness [58]. However, the composite response of LST and DLC film is not usually comfortable during the friction and wear behavior by some working conditions, such as contact pressure, temperature [19], texture geometry [36], and lubricated medium [59]. Further, the combined investigation of LST and DLC film is far from the

universal conclusion for different engineering applications, although these works have been conducted by enough research teams [19,34–37,60–63]. Note that the order of surface texturing and DLC coating is different, and most of these investigations are conducted on the textured surface of DLC coating samples. For carbon steel samples, micro-cracking that results from tensile stress tends to occur within the smooth surface during sliding motion [64]. As known, micro-cracks are usually a bad sign of delamination wear, which consists of several basic steps, such as plastic deformation of the subsurface layer, subsurface crack nucleation, propagation, and generation of loose wear sheets [65]. Obviously, it is a fact that subsurface deformations, void elongation, and crack formation in medium-carbon steel are detrimental to the mating part and should be avoided by taking any surface protection measures. Thus, surface treatments, such as coating and texturing, are better methods of improving the tribological performance and properties of mechanical components [34,63,66], resulting in a clear difference in the worn surfaces after friction and wear experiments (see Figures 10 and 11).

After the LST, the hardness of the surface is enhanced by the laser action, while the substrate material of the counterpart is soft. Thus, both the laser-textured and non-textured zones of the contact surfaces of the friction couple will be in a mess due to frequent plowing and heating effects during the friction process. This results in the active surface been in the inhomogeneous state without harmonized interaction with each other, leading to heat accumulation, which enhances oxidation and friction. Lastly, as oxidation is exacerbated, the sheet scuff peels off, causing serious wear and tear. Conversely, apart from the solid film for the friction reduction of coating surfaces under the lean oil condition, soft carbon coatings undergo the action of plowing and squeezing mechanisms, and the surface roughness changes by the process of scratching and penetration concurrently. This generates new debris, which brings some additional mechanisms of friction and wear [67]. Differently, hard coating usually affects the load-carrying capacity through coating strength and substrate deformation [68]. Throughout the contact, the reduction of the actual area and the interlocking materials affects chiefly the surface roughness, while the asperity fatigue leads to the generation of wear debris. The bearing capacity and wear resistance of friction pairs under lubrication conditions can be improved by the hydrodynamic lubrication, micro-oil pool effect, and micro-lubrication of LST technology. At the same time, the tribological properties of friction couples under dry friction, and the boundary lubrication conditions can be enhanced by DLC coating. Through the coupling and synergy of these two mechanisms, comprehensive tribological properties of friction pairs can be improved, and the working conditions and application fields of specific friction pairs can be expanded. Thereafter, the lubrication design principle of the textured surface with carbon coating is illustrated and shown in Figure 16.

The wear traces shown by SEM photographs indicate different wear mechanisms for the different friction pairs with various treated surfaces. Specifically, the textured surface with coating presents oxidative and adhesive wear mechanism under starved lubrication conditions. The oxidation is not an incomprehensible result because amorphous carbon film cannot hold stable inertia at a fairly high temperature. The flashing temperature may get to hundreds Centigrade owing to the micro-contact with a heavy load during the dry friction condition. Thus, local carbonization occurs at the actual zone rather than the apparent region. Additionally, carbon film has certain mobility during micro-plowing and micro-cutting, which are micro-abrasive mechanisms of generating wear and material migration. Superficially, it is undesirable to improve the abrasion resistance of the working surface with micro-pits and carbon film. However, the truth of the matter is quite different because the periodic temperature rise may be higher in starved friction. Consequently, the carbon film is softened occasionally, and sound solid lubrication might well be realized, with no great loss of the bulk material and the counterpart after friction. Moreover, diamond and diamond-like carbon cannot produce protective oxide layers with oxidation and volatile CO<sub>2</sub>. Additionally, for diamond-like carbon, H<sub>2</sub>O is formed, which will emerge at the oxidation temperature [46], and a water-mediated hydrogen diffusion mechanism may exist on the oxide surface at a normal temperature or less.

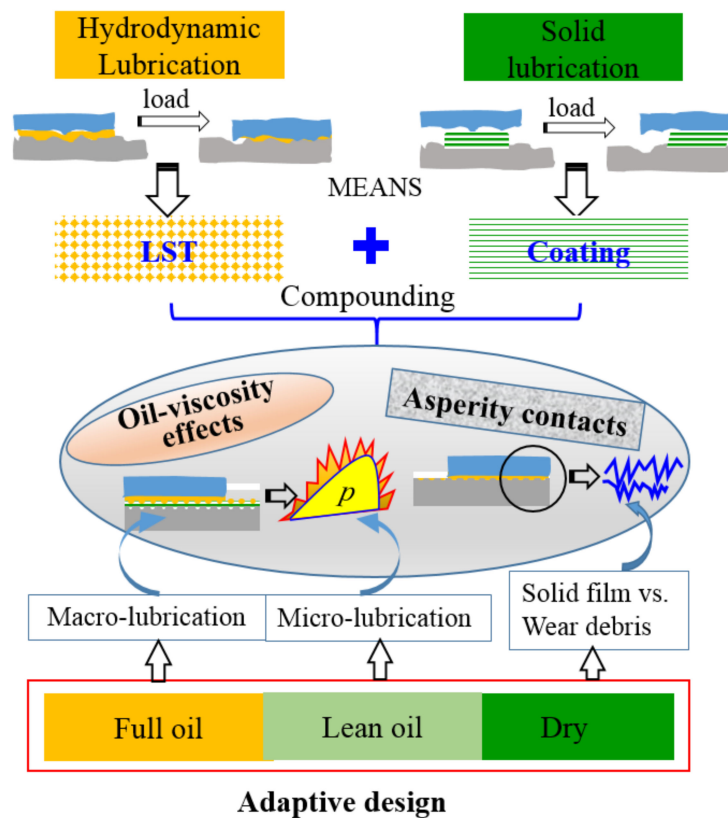


**Figure 16.** Illustration of the laser-textured surfaces for lubrication adaptive design.

Surface roughness is an important factor in scuffing failure, whether it occurs under conditions of boundary lubrication or mixed lubrication [48]. In this study, the surface of the bulk materials is not very smooth with some initial defects, which might have affected the result of the test. The micro-pits array of the laser-textured surfaces contains an error in depth and profile induced by the laser pulses. In addition, it is not easy to design the thickness of the carbon film to get an excellent tribological performance. A fairly thin film would lose its effects in dry and starved conditions, whereas a thick film would rather weaken the interface characteristic of the textured surface contact resistance and heat transfer. Moreover, the friction coefficients for several surfaces under starved conditions are not available, which are constrained by the weak resistance to shock for torque sensors. Consequent upon these problems and oversights, friction and wear behaviors carried out are quantitative to an extent, accompanied by qualitative analysis. This result could not be set aside without a grave responsibility for tribological performances and behaviors. Surface oxidization and van der Waals attractive energy over the carbon structures with nanoscale conformity [69] lead to a novel, critical, and unfolding surface treatment, yet some sagging problems with physicochemical actions demand further study.

## 5. Conclusions

This study illustrated the tribological performances of a laser-textured surface combined with carbon coatings compared with three typical surfaces (smooth surface, textured surface, and coated surface). The advantages of the textured surface with coating were demonstrated by surface characterization and tribological tests on a ring-on-ring rig. The analyzed results made us understand the relationship between material properties, surface topographies, and tribological behavior, as outlined below.

(1) Engineering surfaces after texturing and coating could be characterized using classical roughness and Abbott–Firestone parameters. Worn regions were isotropic in the horizontal (parallel to the sliding direction) and vertical directions. Changes in surface topography of worn traces were related to the wear behaviors and friction mechanism.

(2) Laser-textured surfaces with carbon coating significantly improved the friction and wear properties of the 45 steel under lubricated conditions, by consistently maintaining a steady-state friction coefficient. Comparing to the smooth surface, the stable friction coefficient under lubricated conditions (medium speed and load) of the textured surface, coated surface, and textured and coated surface were reduced by 17%, 41%, and 59%, respectively.

(3) The trend of temperature rise of the textured surface with coating was not consistent with that of the friction coefficient under different working conditions, which has accounted for the significant difference in the influence of the degree of working conditions (i.e., speed and load) on the friction coefficient and temperature rise.

(4) Under lubricated conditions, the plowing friction was weakened by the viscous shearing of lubricating oil, and the micro-cracks in the perpendicular direction of the sliding motion were present. The textured surface with a coating underwent the plowing friction accompanied by corrosion and adhesive wear under the conditions of high-speed and light load.

(5) Diamond-like carbon films, combined with microscopic bearing and pooling effects of surface textures, could significantly improve the hydrodynamic lubrication performance, whereas the available solid lubrication was available by the formation of low friction film under dry friction conditions. The additional effect provided a basis and scheme for lubrication adaptive design under complex working conditions.

**Author Contributions:** Conceptualization, Y.Z. and X.H.; methodology, Y.Z.; software, H.F.; validation, X.W., H.L., and X.X.; formal analysis, X.W.; investigation, H.F.; resources, Y.F.; data curation, J.J.; writing—original draft preparation, Y.Z.; writing—review and editing, J.C.P.; visualization, Y.Z.; supervision, X.H.; project administration, Y.F.; funding acquisition, Y.Z., H.F., X.W., H.L., and X.H. All authors have read and agreed to the published version of the manuscript.

**Funding:** This research was funded by the National Natural Science Foundation of China, grant No. 51705210, 51705211, 51705101, 51975252; Jiangsu Province Post-Doctoral Research Funding Scheme, grant No. 2019K195, 2019K233; State Key Laboratory of Mechanical System and Vibration Research Fund, grant No. MSV-2019-17; Key Laboratory of Micro-Systems and Micro-Structures Manufacturing (Harbin Institute of Technology), Ministry of Education, grant No. 2019KM009; Fundamental Research Funds for the Central Universities grant No. HIT.NSRIF.2020043. The APC was funded by the Fundamental Research Funds for the Central Universities, grant No. 2020043.

**Conflicts of Interest:** The authors declare no conflict of interest.

## References

1. Gualtieri, E.; Borghi, A.; Calabri, L.; Pugno, N.; Valeri, S. Increasing nanohardness and reducing friction of nitride steel by laser surface texturing. *Tribol. Int.* **2009**, *42*, 699–705. [[CrossRef](#)]
2. Spikes, H. Tribology research in the twenty-first century. *Tribol. Int.* **2001**, *34*, 789–799. [[CrossRef](#)]
3. Holmberg, K.; Andersson, P.; Erdemir, A. Global energy consumption due to friction in passenger cars. *Tribol. Int.* **2012**, *47*, 221–234. [[CrossRef](#)]
4. Rabuté, R.; Tian, T. Challenges involved in piston top ring designs for modern SI engines. *J. Eng. Gas Turbines Power* **2001**, *123*, 448–459. [[CrossRef](#)]
5. Arslan, A.; Quazi, M.M.; Masjuki, H.H.; Kalam, M.A.; Varman, M.; Zulkifli, N.W.M.; Jamshaid, M.; Mandalan, S.M.; Gohar, G.A.; Gulzar, M.; et al. Wear characteristics of patterned and un-patterned tetrahedral amorphous carbon film in the presence of synthetic and bio based lubricants. *Mater. Res. Express* **2018**, *6*, 036414. [[CrossRef](#)]
6. Wang, X.; Khonsari, M.; Li, S.; Dai, Q.; Wang, X. Experimental verification of textured mechanical seal designed using multi-objective optimization. *Ind. Lubr. Tribol.* **2019**, *71*, 766–771. [[CrossRef](#)]
7. Trdan, U.; Hocevar, M.; Gregorcic, P. Transition from superhydrophilic to superhydrophobic state of laser textured stainless steel surface and its effect on corrosion resistance. *Corros. Sci.* **2017**, *123*, 21–26. [[CrossRef](#)]
8. Etsion, I. State of the art in laser surface texturing. *J. Tribol.* **2005**, *127*, 248–253. [[CrossRef](#)]
9. Etsion, I.; Sher, E. Improving fuel efficiency with laser surface textured piston rings. *Tribol. Int.* **2009**, *42*, 542–547. [[CrossRef](#)]

10. Ronen, A.; Etsion, I.; Kligerman, Y. Friction-reducing surface-texturing in reciprocating automotive components. *Tribol. Trans.* **2001**, *44*, 359–366. [[CrossRef](#)]
11. Shinkarenko, A.; Kligerman, Y.; Etsion, I. The effect of elastomer surface texturing in soft elasto-hydrodynamic lubrication. *Tribol. Lett.* **2009**, *36*, 95–103. [[CrossRef](#)]
12. Antoszewski, B. Mechanical seals with sliding surface texture—model fluid flow and some aspects of the laser forming of the texture. *Procedia Eng.* **2012**, *39*, 51–62. [[CrossRef](#)]
13. Shi, L.; Wang, X.; Su, X.; Huang, W.; Wang, X. Comparison of the load-carrying performance of mechanical gas seals textured with microgrooves and microdimples. *J. Tribol.* **2016**, *138*, 021701. [[CrossRef](#)]
14. Lu, X.; Khonsari, M. An experimental investigation of dimple effect on the Stribeck curve of journal bearings. *Tribol. Lett.* **2007**, *27*, 169. [[CrossRef](#)]
15. Brizmer, V.; Kligerman, Y. A laser surface textured journal bearing. *J. Tribol.* **2012**, *134*, 031702. [[CrossRef](#)]
16. Sulaiman, M.H.; Christiansen, P.; Bay, N. The Influence of Tool Texture on Friction and Lubrication in Strip Reduction Testing. *Lubricants* **2017**, *5*, 3. [[CrossRef](#)]
17. Fang, S.; Llanes, L.; Bähre, D. Wear Characterization of Cemented Carbides (WC–CoNi) Processed by Laser Surface Texturing under Abrasive Machining Conditions. *Lubricants* **2017**, *5*, 20. [[CrossRef](#)]
18. Sharma, V.; Pandey, P.M. Geometrical design optimization of hybrid textured self-lubricating cutting inserts for turning 4340 hardened steel. *Int. J. Adv. Manuf. Technol.* **2017**, *89*, 1575–1589. [[CrossRef](#)]
19. Arslan, A.; Masjuki, H.H.; Varman, M.; Kalam, M.A.; Quazi, M.M.; Mosarof, M.H. Effect of change in temperature on the tribological performance of micro surface textured DLC coating. *J. Mater. Res.* **2016**, *31*, 1837–1847. [[CrossRef](#)]
20. Ling, T.D.; Liu, P.; Xiong, S.; Grzina, D.; Cao, J.; Wang, Q.J.; Xia, Z.C.; Talwar, R. Surface texturing of drill bits for adhesion reduction and tool life enhancement. *Tribol. Lett.* **2013**, *52*, 113–122. [[CrossRef](#)]
21. Grabon, W.; Koszela, W.; Pawlus, P.; Ochwat, S. Improving tribological behaviour of piston ring–cylinder liner, frictional pair by liner surface texturing. *Tribol. Int.* **2013**, *61*, 102–108.
22. Gu, C.; Meng, X.; Xie, Y.; Yang, Y. Effects of surface texturing on ring/liner friction under starved lubrication. *Tribol. Int.* **2016**, *94*, 591–605.
23. Baumgart, P.; Krajnovich, D.; Nguyen, T.; Tam, A.G. A new laser texturing technique for high performance magnetic disk drives. *IEEE Trans. Magn.* **1995**, *31*, 2946–2951.
24. Oka, T.; Itani, K.; Taguchi, Y.; Nagasaka, Y. Development of interferometric excitation device for micro optical diffusion sensor using laser-induced dielectrophoresis. *J. Microelectromech. Syst.* **2012**, *21*, 324–330.
25. Yu, H.; Wang, X.; Zhou, F. Geometric shape effects of surface texture on the generation of hydrodynamic pressure between conformal contacting surfaces. *Tribol. Lett.* **2010**, *37*, 123–130.
26. Akbarzadeh, S.; Khonsari, M. Effect of surface pattern on Stribeck curve. *Tribol. Lett.* **2010**, *37*, 477–486.
27. Kovalchenko, A.; Ajayi, O.; Erdemir, A.; Fenske, G.; Etsion, I. The effect of laser surface texturing on transitions in lubrication regimes during unidirectional sliding contact. *Tribol. Int.* **2005**, *38*, 219–225.
28. Kot, M.; Major, Ł.; Lackner, J.; Chronowska-Przywara, K.; Janusz, M.; Rakowski, W. Mechanical and tribological properties of carbon-based graded coatings. *J. Nanomater.* **2016**, *51*, 1–14.
29. Holmberg, K.; Mathews, A. Coatings tribology: A concept, critical aspects and future directions. *Thin Solid Films* **1994**, *253*, 173–178.
30. Tyagi, A.; Walia, R.; Murtaza, Q.; Pandey, S.M.; Tyagi, P.K.; Bajaj, B. A critical review of diamond like carbon coating for wear resistance applications. *Int. J. Refract. Met. Hard Mater.* **2019**, *78*, 107–122.
31. Wang, J.; Ma, J.; Huang, W.; Wang, L.; He, H.; Liu, C. The investigation of the structures and tribological properties of F-DLC coatings deposited on Ti-6Al-4V alloys. *Surf. Coat. Technol.* **2017**, *316*, 22–29. [[CrossRef](#)]
32. Han, X.; Zheng, J.; Hao, J.; Zhang, S. The microstructure, mechanical and tribological properties of aC: H films with self-assembled carbon nanohoops. *Surf. Coat. Technol.* **2017**, *311*, 27–34. [[CrossRef](#)]
33. Charitidis, C. Nanomechanical and nanotribological properties of carbon-based thin films: A review. *Int. J. Refract. Met. Hard Mater.* **2010**, *28*, 51–70. [[CrossRef](#)]
34. Arslan, A.; Masjuki, H.H.; Kalam, M.A.; Varman, M.; Mosarof, M.H.; Mufti, R.A.; Quazi, M.M.; Khuong, L.S.; Liaqat, M.; Jamshaid, M.; et al. Investigation of laser texture density and diameter on the tribological behavior of hydrogenated DLC coating with line contact configuration. *Surf. Coat. Technol.* **2017**, *322*, 31–37. [[CrossRef](#)]
35. Yasumaru, N.; Miyazaki, K.; Kiuchi, J. Control of tribological properties of diamond-like carbon films with femtosecond-laser-induced nanostructuring. *Appl. Surf. Sci.* **2008**, *254*, 2364–2368. [[CrossRef](#)]

36. Chouquet, C.; Gavillet, J.; Ducros, C.; Sanchette, F. Effect of DLC surface texturing on friction and wear during lubricated sliding. *Mater. Chem. Phys.* **2010**, *123*, 367–371. [[CrossRef](#)]
37. Ding, Q.; Wang, L.; Hu, L.; Hu, T.Y. The pairing-dependent effects of laser surface texturing on micro tribological behavior of amorphous carbon film. *Wear* **2012**, *274–275*, 43–49. [[CrossRef](#)]
38. Shamsul Baharin, A.F.; Ghazali, M.J.A.; Wahab, J. Laser surface texturing and its contribution to friction and wear reduction: A brief review. *Ind. Lubr. Tribol.* **2016**, *68*, 57–66. [[CrossRef](#)]
39. Fu, Y.; Liu, Q.; Ye, Y.; Hua, X.; Kang, Z.; Hao, F. Research on Laser Surface Micro Texturing Processing of Single Pulse Intervals. *Chin. J. Lasers* **2015**, *42*, 1203005.
40. Fu, Y.; Pan, G.; Hua, X.; Fu, H.; Gao, X. Study on the laser micro-manufacturing equipment of special micro-manufacturing technology. In Proceedings of the 2011 Second International Conference on Digital Manufacturing & Automation, Zhangjiajie, China, 5–7 August 2011; pp. 1176–1179.
41. Dutta Majumdar, J.I. Laser material processing. *Int. Mater. Rev.* **2011**, *56*, 341–388. [[CrossRef](#)]
42. Hu, T.; Hu, L.; Ding, Q. Effective solution for the tribological problems of Ti-6Al-4V: Combination of laser surface texturing and solid lubricant film. *Surf. Coat. Technol.* **2012**, *206*, 5060–5066. [[CrossRef](#)]
43. Moore, A.J.W.; Tegart, W.J.M.; Bowden, F.P. Relation between friction and hardness. *Proc. R. Soc. Lond. Ser. A Math. Phys. Sci.* **1952**, *212*, 452–458.
44. Sahoo, P.; Ali, S.M. Elastic-plastic adhesive contact of rough surfaces with soft coatings. *Tribol. Online* **2008**, *3*, 216–221. [[CrossRef](#)]
45. Vandeveld, T.C.S.; Vandierendonck, K.; Van Stappen, M.; Du Mong, W.; Perremans, P. Cutting applications of DLC, hard carbon and diamond films. *Surf. Coat. Technol.* **1999**, *113*, 80–85. [[CrossRef](#)]
46. Habig, K.H. Fundamentals of the tribological behaviour of diamond, diamond-like carbon and cubic boron nitride coatings. *Surf. Coat. Technol.* **1995**, *76*, 540–547. [[CrossRef](#)]
47. Andersson, J.; Erck, R.A.; Erdemir, A. Friction of diamond-like carbon films in different atmospheres. *Wear* **2003**, *254*, 1070–1075. [[CrossRef](#)]
48. Horng, J.H. Contact analysis of rough surfaces under transition conditions in sliding line lubrication. *Wear* **1998**, *219*, 205–212. [[CrossRef](#)]
49. Jianglong, L.; Zhirong, Z. A study of morphologies of residual austenite after laser transformation hardening. *Mater. Mech. Eng.* **1989**, *13*, 35–38. (In Chinese)
50. Ling, Z. The microstructure and the wear resistance of 45-steel after laser transformation hardening. *J. Chongqing Jiaotong Inst.* **1992**, *11*, 103–107. (In Chinese)
51. Jiandong, H.; Zhang, L. The observation on the lath martensite in the laser processing areas by TEM. *J. Chin. Electron. Microsc. Soc.* **1986**, *5*, 72–76. (In Chinese)
52. We, F.; Zhiqin, Y. Study on laser transformation hardening of metal surface. *Heat Treat. Met.* **1982**, *25*, 12–20. (In Chinese)
53. Grabon, W.A. A new approach to the description of height distribution of plateau honed cylinder liner surface texture during the initial stage of wear. *Wear* **2018**, *408*, 34–42. [[CrossRef](#)]
54. Moriguchi, H.; Ohara, H.; Tsujioka, M. History and applications of diamond-like carbon manufacturing processes. *Sci Tech. Rev.* **2016**, *82*, 52–58.
55. Kalin, M.; Velkavrh, I.; Vižintin, J. The Stribeck curve and lubrication design for non-fully wetted surfaces. *Wear* **2009**, *267*, 1232–1240. [[CrossRef](#)]
56. Podgornik, B.; Jacobson, S.; Hogmark, S. DLC coating of boundary lubricated components—Advantages of coating one of the contact surfaces rather than both or none. *Tribol. Int.* **2003**, *36*, 843–849. [[CrossRef](#)]
57. Topolovec-Miklozic, K.; Lockwood, F.; Spikes, H. Behaviour of boundary lubricating additives on DLC coatings. *Wear* **2008**, *265*, 1893–1901. [[CrossRef](#)]
58. Kovaci, H.; Yetim, A.F.; Baran, O.; Celik, A. Tribological behavior of DLC films and duplex ceramic coatings under different sliding conditions. *Ceram. Int.* **2018**, *44*, 7151–7158. [[CrossRef](#)]
59. Peng, R.; Zhang, P.; Tian, Z.; Zhu, D.; Chen, C.; Yin, B.; Hua, X. Effect of textured DLC coatings on tribological properties of titanium alloy under grease lubrication. *Mater. Res. Express* **2020**, *7*, 066408. [[CrossRef](#)]
60. Amanov, A.; Watabe, T.; Tsuboi, R.; Sasaki, S. Improvement in the tribological characteristics of Si-DLC coating by laser surface texturing under oil-lubricated point contacts at various temperatures. *Surf. Coat. Technol.* **2013**, *232*, 549–560. [[CrossRef](#)]
61. Shum, P.W.; Zhou, Z.F.; Li, K.Y. To increase the hydrophobicity, non-stickiness and wear resistance of DLC surface by surface texturing using a laser ablation process. *Tribol. Int.* **2014**, *78*, 1–6. [[CrossRef](#)]

62. Arslan, A.; Masjuki, H.H.; Varman, M.; Kalam, M.A.; Quazi, M.M.; Al Mahmud, K.A.H.; Gulzar, M.; Habibullah, M. Effects of texture diameter and depth on the tribological performance of DLC coating under lubricated sliding condition. *Appl. Surf. Sci.* **2015**, *356*, 1135–1149. [[CrossRef](#)]
63. He, D.; Zheng, S.; Pu, J.; Zhang, G.; Hu, L. Improving tribological properties of titanium alloys by combining laser surface texturing and diamond-like carbon film. *Tribol. Int.* **2015**, *82*, 20–27. [[CrossRef](#)]
64. Gu, D.; Hagedorn, Y.C.; Meiners, W.; Meng, G.; Batista, R.J.S.; Wissenbach, K.; Poprawe, R. Densification behavior, microstructure evolution, and wear performance of selective laser melting processed commercially pure titanium. *Acta Mater.* **2012**, *60*, 3849–3860. [[CrossRef](#)]
65. Suh, N.P. An overview of the delamination theory of wear. *Wear* **1977**, *44*, 1–16. [[CrossRef](#)]
66. Dufils, J.; Faverjon, F.; Heau, C.; Donnet, C.; Benayoun, S.; Valette, S. Combination of laser surface texturing and DLC coating on PEEK for enhanced tribological properties. *Surf. Coat. Technol.* **2017**, *329*, 29–41. [[CrossRef](#)]
67. Aghababaei, R. On the origins of third-body particle formation during adhesive wear. *Wear* **2019**, *426–427*, 1076–1081. [[CrossRef](#)]
68. Wang, C.T.; Hakala, T.J.; Laukkanen, A.; Ronkainen, H.; Holmberg, K.; Gao, N.; Wood, R.J.; Langdon, T.G. An investigation into the effect of substrate on the load-bearing capacity of thin hard coatings. *J. Mater. Sci.* **2016**, *51*, 4390–4398. [[CrossRef](#)]
69. Bhaskaran, H.; Gotsmann, B.; Sebastian, A.; Drechsler, U.; Lantz, M.A.; Despont, M.; Jaroenapibal, P.; Carpick, R.W.; Chen, Y.; Sridharan, K. Ultralow nanoscale wear through atom-by-atom attrition in silicon-containing diamond-like carbon. *Nat. Nanotechnol.* **2010**, *5*, 181–185. [[CrossRef](#)]



© 2020 by the authors. Licensee MDPI, Basel, Switzerland. This article is an open access article distributed under the terms and conditions of the Creative Commons Attribution (CC BY) license (<http://creativecommons.org/licenses/by/4.0/>).